

An effective theory of collective deep learning

Lluís Arola-Fernández* and Lucas Lacasa†

*Instituto de Física Interdisciplinar y Sistemas Complejos IFISC (CSIC-UIB),
Campus UIB, 07122 Palma de Mallorca, Spain*

(Dated: October 20, 2023)

Unraveling the emergence of collective learning in systems of coupled artificial neural networks is an endeavor with broader implications for physics, machine learning, neuroscience and society. Here we introduce a minimal model that condenses several recent decentralized algorithms by considering a competition between two terms: the local learning dynamics in the parameters of each neural network unit, and a diffusive coupling among units that tends to homogenize the parameters of the ensemble. We derive the coarse-grained behavior of our model via an effective theory for linear networks that we show is analogous to a deformed Ginzburg-Landau model with quenched disorder. This framework predicts (depth-dependent) disorder-order-disorder phase transitions in the parameters' solutions that reveal the onset of a collective learning phase, along with a depth-induced delay of the critical point and a robust shape of the microscopic learning path. We validate our theory in realistic ensembles of coupled nonlinear networks trained in the MNIST dataset under privacy constraints. Interestingly, experiments confirm that individual networks –trained only with private data– can fully generalize to unseen data classes when the collective learning phase emerges. Our work elucidates the physics of collective learning and contributes to the mechanistic interpretability of deep learning in decentralized settings.

Collective behavior emerging from the dynamics of many interacting particles or units is the flagship of complexity [1–3] and a common feature found across natural and artificial complex systems [4–6]. Learning, a paradigmatic example of collective behavior [7, 8], is a fascinating ability of the brain, where large ensembles of neurons interact, adapting their synaptic circuits in such a way that allow us to learn from experience. Learning can also occur in a collective manner among interacting agents that learn from each other, and at different scales, from ant colonies [5] to social communities [9] or robot swarms [10]. Such generality and multiscale nature of learning has attracted a great interest across fields, from neuroscience and sociology to theoretical physics and computer science, and the major advances in the problem have definitely benefited from this cross-disciplinary research. In fact, ideas from complex systems and statistical physics are at the roots of the early models of computation in neural networks [11] and in classical machine learning tools such as random forests and particle swarm optimization [12], among other notable contributions [13–19]. The many-particle approach has proved particularly successful in deep learning [20], a collection of algorithms and techniques involving very large and overparametrized neural networks, which has recently shown astonishing results in a myriad of challenging tasks [21, 22] and intriguing emerging behavior in large language models [23].

Interestingly, industry-related constraints posed by e.g. data privacy issues and power consumption during training [24, 25], along with the perpetual quest for finding learning architectures with enhanced performance, have driven the field of machine learning to explore new solu-

tions that, in hindsight, seem to capitalize on some form of collective behavior [17, 20]. These range from ensemble approaches [26, 27] to other decentralized solutions [24, 28] including federated learning [25, 28, 29], cooperative learning [30] or transfer learning [31]. These notable engineering successes provide a strong motivation to understand, from a principled complex-systems viewpoint, whether collections of ‘interacting brains’ –rather than ‘interacting neurons’– do indeed develop collective behavior in the physical sense [5, 17], i.e. whether agents learning solely from local data have a collective advantage when coupled along the learning process (the whole being more than the sum of its parts [1]). Does collective learning emerge when (local) neural networks are put in interaction? Does this collective learning phase emerge abruptly –as in the theory of phase transitions–? And do local deep learning architectures play a non-trivial role in such phenomenology? Below we provide affirmative answers to all these questions. We present a minimal mathematical model of collective learning where we show that local brains solely trained for isolated tasks (private data) are capable to generalize far outside their training set when coupled, and this happens via the onset of a collective learning phase transition. Our results are predicted by a physical effective theory (amenable to mechanistic interpretability [13–16]) and subsequently confirmed in a range of realistic experiments.

Collective learning model – Our proof of concept will be evaluated on a classification task to be solved by a coupled ensemble of *vanilla* feed-forward neural networks, where each neural network is trained using data from a single class and evaluation is performed on the whole (multiclass) test set. However, the framework introduced below is flexible and extends to a generic supervised task or neural architecture. Following a standard parametrization [32], let $\mathcal{D} = \{(\mathbf{x}, \mathbf{y})\} \subseteq \mathbb{R}^{n_0} \times \mathbb{R}^{n_{D+1}}$

* lluisarolaf@gmail.com

† lucas@ifisc.uib-csic.es

denote the training set, where $\mathcal{X} = \{\mathbf{x} : (\mathbf{x}, \mathbf{y}) \in \mathcal{D}\}$ and $\mathcal{Y} = \{\mathbf{y} : (\mathbf{x}, \mathbf{y}) \in \mathcal{D}\}$ denote the input and output (labels) vectors with dimension n_0 and n_{D+1} , respectively. The training data is partitioned and distributed across N neural units (the local models), such that $\mathcal{D} = \cup_{i=1}^N \mathcal{D}_i$. Each local model is a fully-connected feed-forward deep network with D hidden layers with widths n_d , for $d = 1, \dots, D$, a readout (output) layer with n_{D+1} neurons, and nonlinear activation functions in the hidden neurons. We define $\bar{\mathbf{y}} = f_i(\mathbf{x}, \boldsymbol{\theta}_i)$ as the predicted output value given the input \mathbf{x} and the set of trainable parameters $\boldsymbol{\theta}_i = \{\theta_i^\alpha\}$, where α runs over all parameter of the i -th unit. We consider a learning process under privacy constraints, such that each neural unit seeks to minimize the local empirical loss function

$$\mathcal{L}_i = \sum_{(\mathbf{x}_i, \mathbf{y}_i) \in \mathcal{D}_i} \ell[f(\mathbf{x}_i, \boldsymbol{\theta}_i), \mathbf{y}_i] + \gamma \|\boldsymbol{\theta}_i\|_2, \quad (1)$$

where the sum runs over the data tuples associated to the i -th unit. The individual loss function $\ell(\bar{\mathbf{y}}, \mathbf{y}_i) : \mathbb{R}^{n_{D+1}} \times \mathbb{R}^{n_{D+1}} \rightarrow \mathbb{R}$, measures the error between the prediction on a single data point and the corresponding true value (or label) and the right-hand term is a standard weight decay (L_2 regularization) with strength γ that encourages a lower model complexity, improving generalization [17, 20]. To minimize Eq.(1), the Backpropagation algorithm tunes the parameters of the N units efficiently via Stochastic Gradient Descent (SGD) [20] (see Methods for details). Since local learning is restricted to the private data assigned to each unit, we introduce an interaction mechanism to induce collective learning in the system, as explained in Fig. 1. As a minimal mechanism, we select a consensus-based model [30], where units are diffusively coupled in a relation ‘parameter-to-parameter’. The interaction links (and their intensities) are captured by the weighted adjacency matrix $Q \in \mathbb{R}^{N \times N} = \{q_{ij}\}$ of the supra-network. Combining both local and interaction terms, each of the α parameters of the i -th unit is updated at each iteration following

$$\theta_i^\alpha(t+1) = \theta_i^\alpha(t) - \eta \nabla_{\theta_i^\alpha} \mathcal{L}_i + \frac{\eta \sigma}{N} \sum_{j=1}^N q_{ij} [\theta_j^\alpha(t) - \theta_i^\alpha(t)], \quad (2)$$

where η is the learning rate and σ the coupling strength of the interactions. To assess collective learning, we let the dynamics relax to a stationary state (when parameters cease to evolve), and then evaluate the mean test loss, i.e. the local loss evaluated with global (multiclass) test data $\mathcal{D}^{\text{test}}$, averaged over the units

$$\langle L \rangle = \frac{1}{N} \sum_{i=1}^N \sum_{(\mathbf{x}, \mathbf{y}) \in \mathcal{D}^{\text{test}}} \ell[f(\mathbf{x}, \boldsymbol{\theta}_i), \mathbf{y}], \quad (3)$$

which serves as an order parameter that measures the collective performance of the system. In classification tasks with a discrete number of classes (as in the MNIST

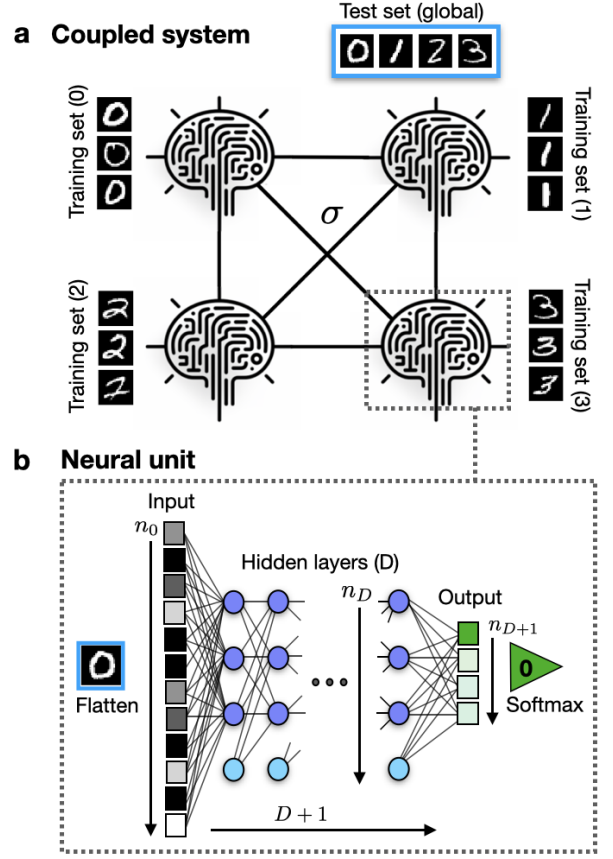


FIG. 1. Collective learning in coupled neural networks: Toy example. **a:** Small mean-field network of $N = 4$ coupled neural units trained with private data classes of MNIST, interacting with coupling strength σ . **b:** Simplified representation of the deep feed-forward architecture of a local neural unit (solely trained with digit-3 images). A test point far outside the training set (here, a digit-0 image) is flattened as an input and processed towards the output layer. In this example, the neural unit predicts well an unseen class during training due to a collective learning mechanism emerging from the interactions.

problem), one is also interested in evaluating the accuracy metric $\langle A \rangle$ that measures the percentage of correct class predictions in the test set, where the brackets indicate again an average over the neural units in the ensemble. We expect $\langle L \rangle$ ($\langle A \rangle$) to be low (high) if neural units are able to generalize outside their training set – a fingerprint of collective learning –, and remain high (low) otherwise. To capture the microscopic details of the process, we use the cross-loss and cross-accuracy matrices $L_x, A_x \in \mathbb{R}^{N \times N}$, where the entry (i, j) determines the loss (accuracy) of the i -th unit (row) when evaluated on data classes assigned to the j -th unit (column).

Note that the dynamics in Eq.(2) lies in the cooperative learning framework [30], akin to decentralized schemes such as elastic averaging SGD [33] and also captures the spirit of federated learning [29] albeit

with some conceptual differences (mainly that here the self-organized dynamics of the units is independent of a centralized *master* model). Previous results proved the convergence of cooperative and federated schemes [28, 30, 33–38], unveiling that while heterogeneous and private data tend to slow down convergence [38], distributed schemes can find solutions with higher generalization properties [33, 39, 40]. The mechanisms underpinning the onset of emergent collective behavior in coupled neural networks under privacy constraints remain, however, poorly understood.

Coarse-grained theory – We leverage on learning scale separation and results on deep linear networks [16, 41] –that shed light on the landscape of nonlinear networks and the existence of regularization-induced learning phase transitions– to derive a coarse-grained theory describing the dynamics in Eq.(2). It can be shown (see Methods for full derivation) that, under suitable approximations and considering a magnetization-like scalar order parameter m_i (which coarse-grains the parameters of the i -th neural unit), the dynamics of Eq.(2) project onto a reduced system of N coupled differential equations

$$\dot{m}_i = \delta_i m_i^D - m_i^{2D+1} - \hat{\gamma} m_i + \frac{\hat{\sigma}}{N} \sum_{j=1}^N q_{ij} (m_j - m_i), \quad (4)$$

where \dot{m}_i indicates the time derivative, $\hat{\sigma}$ and $\hat{\gamma}$ are effective hyper-parameters (coupling and regularization, respectively), q_{ij} are the entries of the supra-network adjacency matrix and D is the neural depth. The full information on the training set is encapsulated in $\hat{\delta}$, a sequence of scalars $\delta_i = \langle \hat{x}_i \hat{y}_i \rangle$, each of them being a one-dimensional projection of the expected input-output correlation, averaged over the data points assigned to the i -th unit. We build the effective test set by aggregating the private training distributions, such that $\langle \delta \rangle = (1/N) \sum_i \langle \hat{x}_i \hat{y}_i \rangle$. Interestingly, the mean effective loss –evaluated on the test set and averaged over the units– scales with the moments of the magnetization as

$$\langle \hat{L} \rangle \sim \langle m^{2(D+1)} \rangle - 2 \langle \delta \rangle \langle m^{(D+1)} \rangle, \quad (5)$$

up to a constant that only depends on the dataset and can be neglected (see Methods). Our goal is to assess the onset of collective learning by solving Eq.(5) in the stationary regime of Eq.(4). From now on, we take an all-to-all unweighted supra-network (i.e. mean-field) with $q_{ij} = 1, \forall i \neq j$. We shall distinguish three scenarios:

Linear regression ($D = 0$) – When units have no hidden layers, Eq.(4) becomes linear. Its stationary solution ($\dot{m}_i = 0$), found self-consistently, reads

$$m_i^* = \frac{\delta_i + \hat{\sigma} \langle \delta \rangle (1 + \hat{\gamma})^{-1}}{1 + \hat{\gamma} + \hat{\sigma}}. \quad (6)$$

The order parameter $\langle m \rangle = \langle \delta \rangle / (1 + \hat{\gamma})$ is independent of coupling $\hat{\sigma}$, as shown in Fig. 2a (light blue crosses). Increasing $\hat{\sigma}$ only makes the distribution of magnetization

narrower, which translates into a monotonously decreasing loss function, as displayed in Fig. 2b.

Shallow networks ($D = 1$) – Eq.(4) becomes

$$\dot{m}_i = (\delta_i - \hat{\gamma}) m_i - m_i^3 + \frac{\hat{\sigma}}{N} \sum_{j=1}^N (m_j - m_i). \quad (7)$$

Remarkably, this equation is formally identical to the mean-field, multiplicative quenched disorder, zero-temperature version of the Ginzburg-Landau (GL) model (ϕ^4 model) [42–46], traditionally used to explore the critical behavior of condensed-matter systems with impurities under Landau’s free energy approach. The local magnetization m_i or *spin* is the average parameter of our neural unit, whereas the heterogeneous allocation of training data plays the role of multiplicative quenched disorder, i.e., that of the material’s random impurities [42]. Eq.(7) displays a rich phenomenology which can be reinterpreted in the context of our neural system¹: For low coupling $\hat{\sigma}$, units trained with data $\delta_i > \hat{\gamma}$ relax in a double well local potential (with two symmetric stable points at $m_{i,\pm}^* = \pm \sqrt{\delta_i - \hat{\gamma}}$), and units with $\delta_i < \hat{\gamma}$ have a single equilibrium point at $m_i^* = 0$. This distribution produces a disordered state (with $|\langle m \rangle| \approx 0$). At a critical coupling strength, a *symmetry-breaking* mechanism induces a collective ordered phase (with $|\langle m \rangle| > 0$) via a second-order collective phase-transition. For even larger coupling, the system returns to a ‘disordered’ phase (via a reentrant phase-transition [43]), where all units become $m_i^* \approx 0 \forall i$, by means of a *collective regularization* mechanism (when diffusion dominates in Eq.(4)). These disorder-order-disorder phase transitions are visualized in Fig. 2a (blue triangles). Interestingly, the critical behavior of the local magnetization triggers a non-monotonous decay of the effective loss. As shown in Fig. 2b (and inset), the non-monotonous shape delays the transition to the collective learning regime with respect to $D = 0$.

Deep networks ($D > 1$) – In the deep learning realm, Eq.(4) represents an exotic deformation of the GL model –which now can be seen as a ϕ^{2D+2} instead of a ϕ^4 model– with odd powers of the order parameter entering in Landau’s free energy for even neural unit depths D , hence breaking rotational symmetry [46]. Fig. 2a (dark blue circles) shows that disorder-order-disorder transitions are still found for $D = 2$, whereas the non-monotonic behavior of the effective loss is enhanced with respect to the shallow case. This effect translates into a further delay of the transition to the collective learning regime, as observed in Fig. 2b and its inset. The depth-induced delay emerges from a positive feedback between the high non-linearity of Eq.(4) and the evaluation of higher moments in the effective loss of Eq.(5). Furthermore, the increased

¹ We take N large and $\hat{\gamma}$ positive but small to avoid the trivial phase and ensure local learning [16] in the units.

non-linearity of the deep case induces an effective landscape with many local minima. A simple linear stability analysis reveals that $m_i^* = 0$ is always a local minimum, which induces a first-order regularization-induced phase transition at the single unit level (see [16] for details). Indeed, this local bistability gets further amplified at the collective scale. Figs. 2a and 2b show significant deviations between adiabatic (circles) and non-adiabatic (dashed line) protocols, which confirm that for $D > 1$ there is a strong sensitivity to initial conditions and a widespread presence of multistability.

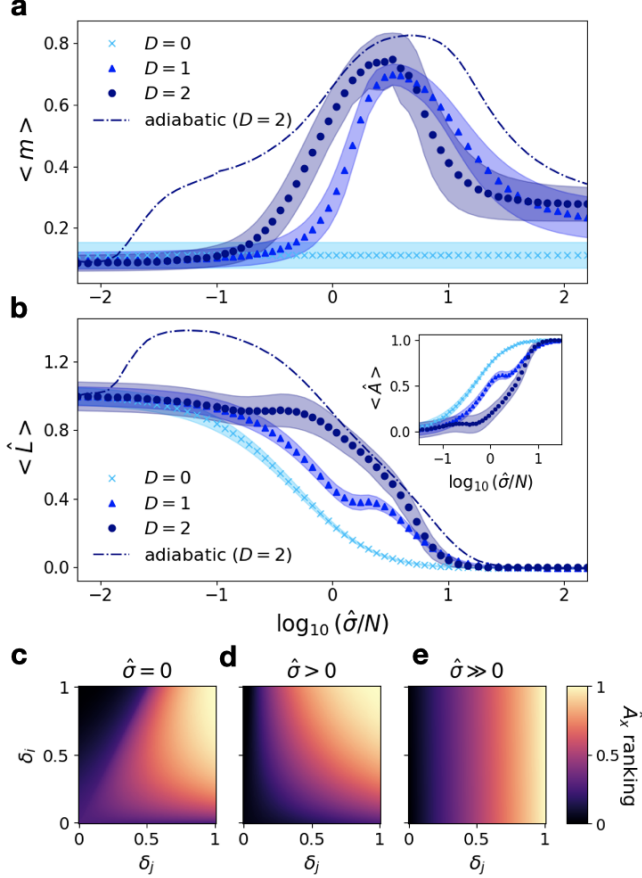


FIG. 2. **Predictions of the effective theory.** **a:** Mean magnetization as a function of coupling strength, for increasing depth (from light to dark blue). The theory predicts disorder-order-disorder transitions in the magnetization for $D > 0$. **b:** Mean effective loss as a function of coupling strength (inset shows $\langle \hat{A} \rangle \approx 1 - \langle \hat{L} \rangle$ in a reduced coupling range). The theory predicts a depth-induced delay in the loss which translates into a delayed critical coupling for the emergence of collective learning ($\langle \hat{A} \rangle > 0$). We use markers for the mean value averaged over initial conditions and quenched sequences (shaded area represents one std.) and dashed lines for the outcome of adiabatic protocols, averaged only over quenched sequences (see Methods). **c:** Ranking of the cross-accuracy matrix \hat{A}_x entries from Eq.(8) in the quenched ‘data’ disorder plane for no coupling, **d:** Medium coupling and **e:** High coupling regimes. See the main text for a discussion and Methods for parametrization details.

Microscopic learning path – We finally leverage our theory to unveil the order in which neural units learn from each other as the system enters the collective learning phase. To tackle this problem analytically, we first construct the cross-loss matrix \hat{L}_x , with $(\hat{L}_x)_{ij} \sim m_i^{D+1}(m_i^{D+1} - 2\delta_j)$. In the uncoupled regime of Eq.(4), we have $m_i(D) \sim m_i(0)^{1/(D+1)}$ and \hat{L}_x can therefore be estimated directly from the $D = 0$ case. We extend this depth-independence as an *ansatz* to the whole coupled regime and compute \hat{L}_x using Eq.(6). Since a high accuracy requires a low loss [20], we use $\hat{A}_x \sim -\hat{L}_x$ to get

$$(\hat{A}_x)_{ij} \sim -\frac{\delta_i + \hat{\sigma}\langle\delta\rangle(1 + \hat{\gamma})^{-1}}{1 + \hat{\gamma} + \hat{\sigma}} \left[\frac{[\delta_i + \hat{\sigma}\langle\delta\rangle(1 + \hat{\gamma})^{-1}]}{1 + \hat{\gamma} + \hat{\sigma}} - 2\delta_j \right]. \quad (8)$$

Eq.(8) presents a rich and interesting structure. Let us set $\gamma, \langle\delta\rangle \rightarrow 0^+$ without loss of generality and evaluate the (normalized) rankings of \hat{A}_{ij} in the positive support of δ . First, in the uncoupled regime we have $(\hat{A}_x)_{ij} \sim 2\delta_i\delta_j - \delta_i^2$ (Fig. 2c), where the approximate diagonal shape indicates that units will have the largest cross-accuracy when evaluated on data δ_j that is similar to their training data δ_i , as expected in the local learning regime. As coupling increases, $(\hat{A}_x)_{ij} \sim (2\delta_i\delta_j + \hat{\sigma}\langle\delta\rangle\delta_j)/(1 + \hat{\sigma})$. The first symmetric term (Fig. 2d) dominates the learning path for a wide range of coupling $\hat{\sigma}$. Instead, for very large coupling (Fig. 2e), the cross-accuracy depends only on the data evaluated, not on the unit making the prediction, as expected when the units become so similar (due to the diffusive coupling) that they make the same predictions and errors. Last, from Eq.(8) we estimate the cumulative cross-accuracy matrix \hat{S}_x to quantify the order in which units learn from each other (i.e. the learning path) as coupling increases. The integral $\hat{S}_x = \int_0^{\hat{\sigma}'} \hat{A}_x d\sigma$ scales, in matrix form, as $\hat{S}_x \sim \log \sigma' \delta \delta^\top + \sigma' \langle\delta\rangle \delta \mathbf{1}^\top$ (where δ^\top is the transpose of the quenched ‘data’ disorder vector and $\mathbf{1}$ is a vector of N ones). Consistent with the low-dimensional nature of our theory, this calculation predicts that the learning path between the units is approximately rank-one, i.e. driven by a single effective dimension (the vector δ). From the previous analysis, the interpretation of δ becomes clear: the higher the δ_j (the stronger the input-output correlation of the j -th data), the faster the units will predict it well (which is amplified if the unit making the predictions is trained with a high δ_i). These findings are reminiscent of how learning works in a single neural network trained with global data [41], which draws an interesting parallel between local and collective scales.

Validation – We now validate the predictions of our effective theory by tackling the standard MNIST image classification task with an ensemble of $N = 10$ nonlinear feed-forward networks (each neural unit is trained solely with images of a unique class, e.g. images of unique digit from 0 to 9). The system learns following the update

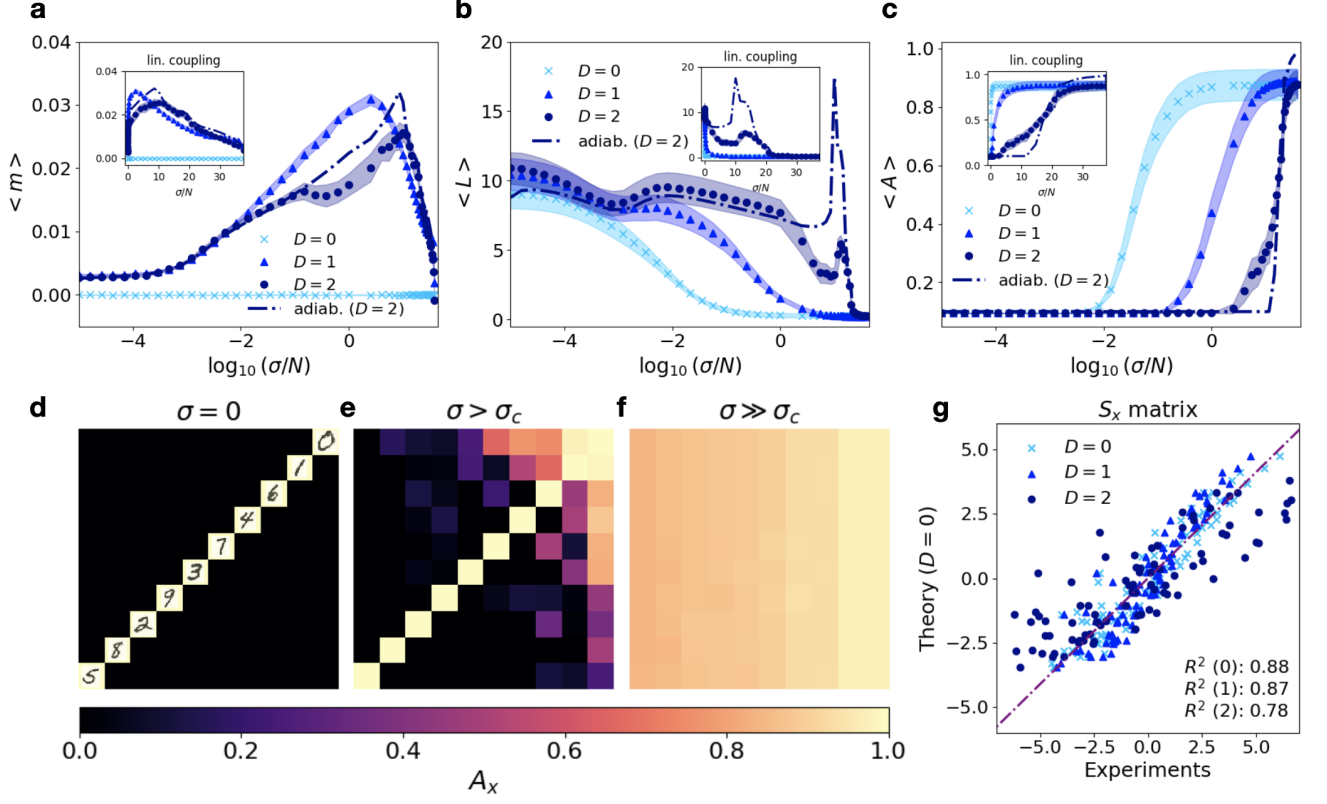


FIG. 3. **MNIST experiments.** **a:** Mean magnetization, **b:** Mean test loss and **c:** Mean test accuracy as a function of coupling strength (in log scale), for depths $D = 0, 1, 2$. The shaded area represents one standard deviation over 20 independent runs and the inset shows the same results in a linear scale of coupling. The dashed line shows results for the adiabatic protocol ($D = 2$). **d:** Empirical cross-accuracy matrix A_x for $D = 1$ averaged over 10 independent realizations at $\sigma/N = 0$, **e:** $\sigma/N = 3$ and **f:** $\sigma/N = 30$. Rows and columns have been ordered from lowest to highest cross-accuracy (the order is indicated by the MNIST digits in **d**) and the y-axis is inverted to facilitate a visual comparison with Fig. 2. **g:** Correlation between the entries of the empirical cumulative cross-accuracy matrix S_x (averaged over 10 runs and shifted by the mean value) for $D = 0, 1, 2$ against the entries of the rank-one truncation of S_x for $D = 0$. We show the coefficient of determination (R^2) for the three cases and the best linear fit as a purple dashed line. See the main text for a discussion and Methods for parametrization details.

rule in Eq.(2), and performance is evaluated on an independent, multiclass test set using Eq.(3) and related metrics (see Methods for details on the implementation). Fig. 3 shows the results for varying neural depth D , across a wide range of coupling values σ and averaging over many realizations of the process. Fig. 3a confirms that, for $D > 0$, disorder-order-disorder phase transitions in the collective order parameter $\langle m \rangle$ appear as coupling increases. As predicted, Fig. 3b shows that the phase transitions induce a non-monotonous behavior of the mean loss, along with a delay of the loss decay to zero (which is amplified with neural depth D). This effect triggers the appearance of a (depth-delayed) critical point where collective learning emerges, as observed in Fig. 3c. The mean accuracy metric grows abruptly from $\langle A \rangle \approx 0.1$ (local learning phase) where units only predict well the class belonging to their private training set, to $\langle A \rangle > 0.1$ at the critical point, up to $\langle A \rangle \approx 1$ (collective learning phase) for larger coupling, where units predict well all classes. Also note that for $D = 2$ the differences

between non-adiabatic (circles) and adiabatic protocols (dashed line) confirm the presence of multistability in the deep case: Intriguingly, the collective learning transition is abruptly delayed when the system has ‘memory’ (i.e. when the parameters are only initialized at $\sigma = 0$). Fig. 3 shows snapshots of the cross-accuracy matrix A_x (for $D = 1$) at three coupling values, reproducing the patterns predicted by our analysis. In **d**: a local phase with an associated diagonal A_x for low coupling (as Fig. 2c), **e**: a symmetric collective learning phase for medium coupling –above the critical point– (as Fig. 2d) and **f**: a column-dependent phase for large coupling², where accuracy only depends on the class that is evaluated (as Fig. 2e). Finally, Fig. 3g displays the empirical correlation between the entries of

² Too much coupling destroys the collective learning phase either by means of the *collective regularization* mechanism, bringing all parameters of each unit to zero, or by an explosion of the diffusion term of Eq.(2) leading to divergences (not shown).

the cumulative cross-accuracy matrix and its rank-one approximation for $D = 0$ (the approximate learning path predicted by the theory) which is computed using the singular value decomposition of S_x and keeping only the leading term. A considerable high R^2 score is sustained for varying depth, providing a quantitative validation of the coarse-grained approach at the microscopic level.

Discussion – While our effective –coarse-grained– theory is based on a list of simplifications and approximations, the predictions about the onset and properties of collective learning are well confirmed on realistic (high-dimensional, highly non-linear) experiments on the MNIST dataset, which supports the mechanistic interpretability of the collective learning paradigm. Yet, much work is required to better understand its rich phenomenology and the relation of decentralized learning schemes with the statistical physics of (deformed) Ginzburg-Landau models. Note that our proof of concept did not cover the myriad of learning phases found in isolated neural networks [15, 47–50], which can get more exotic in the collective case. Extending the effective theory to the complex plane may capture some of these nuances and even increase the analytical tractability (thanks to exact dimensional reductions and other techniques available for coupled oscillators [51–54]). Other promising directions include exploring how the shape and difficulty of a dataset [50] (*effectively* encapsulated in the distribution of quenched disorders) and the supra-network topology [55] (beyond the mean-field, undirected, pair-wise and time-independent case) affect the nature of the phase transitions [56–58], and refining the diffusive coupling mechanism to model heterogeneous neural learners and indirect communication channels [25, 59, 60].

In a nutshell, this work offers a mathematical foundation for collective learning in natural and artificial systems. Our perspective enriches statistical physics approaches to interacting brains [6] and makes a first step towards a next-generation type of physical models [52, 61] to describe emergent social behavior –such as collective learning– in populations of interacting agents. Last, it has not escaped our notice that this framework could contribute to tackle the so-called alignment problem [62] when independent learning models are put in interaction.

METHODS

A. Derivation of the effective equations

We begin by assuming that the learning rate η in Eq.(2) is sufficiently small, such that we can approximate the discrete dynamics by the continuous version

$$\dot{\theta}_i^\alpha = -\nabla_{\theta_i^\alpha} \mathcal{L}_i(\mathbf{x}_i, \mathbf{y}_i, \boldsymbol{\theta}_i, \gamma) + \frac{\sigma}{N} \sum_{j=1}^N a_{ij}(\theta_j^\alpha - \theta_i^\alpha), \quad (9)$$

where $\dot{\theta}_i^\alpha = d\theta_i^\alpha/dt$ is the time-derivative of a parameter, the time step dt in the numerical integration of Eq.(9) corresponds to the learning rate η and bold variables denote vectors (a notation used also in the main text).

Now we follow a common procedure in physics, i.e. to linearize the system and study the properties of the resulting linear approximation [16, 17, 32, 41]. When the choice of $\ell(\hat{y}, y)$ is the mean square error (MSE), the loss function of a deep linear network can be written as [16]

$$\hat{\mathcal{L}}_i = \mathbb{E}_{x_i} \left[\left(\sum_{d_0, \dots, d_{D+1}}^{n_o, \dots, n_{D+1}} [\Theta_{d_{D+1}d_D}^{D+1}]_i \dots [\Theta_{d_1d_0}^1]_i [x_{d_0}]_i - y_i \right)^2 \right] + \gamma \sum_{d=1}^{D+1} \|\Theta_i^d\|_2^2, \quad (10)$$

where $\mathbb{E}_{x_i}[\cdot]$ denotes the expected value over the accessible data points and $\|\Theta_i^d\|_2$ is the squared L_2 norm of all elements in the parameters' matrix of the d -layer. Each sum in the first term of Eq.(10) runs over all the neurons of a given layer with width n_d . The index i is kept to reflect that the loss, the parameters and the data belong to the i -th neural unit in the ensemble setting.

Here we follow the ‘mean-field’ analysis of [16], assuming that both the input and output are one-dimensional, and we approximate each matrix Θ_i^d by the mean value of its entries, a scalar $c_d \hat{\theta}_i^d$, where c_d is a layer-dependent constant that we set to $c_d = 1$ for simplicity here. The loss function of the i -th unit in Eq.(10) then reads as

$$\hat{\mathcal{L}}_i \approx \mathbb{E}_{x_i} \left[\left(\hat{x}_i \prod_{d=1}^{D+1} \hat{\theta}_i^d - \hat{y}_i \right)^2 \right] + \gamma \sum_{d=1}^{D+1} (\hat{\theta}_i^d)^2, \quad (11)$$

where \hat{x}_i and \hat{y}_i are the one-dimensional projections of input and output for a data point assigned to the i -th unit. Under this mean-field approximation, we can reduce the number of coupled equations in Eq.(9) from a very large number (α runs from 1 to the dimension of $\text{vec}(\cup_{d=1}^{D+1} \Theta^d)$) to just $(D+1) \times N$ equations, one for each layer of each unit. In particular, we can now compute the gradient in Eq.(9) with respect to the variable $\hat{\theta}_i^d$, and using the loss function of Eq.(11) we get

$$\dot{\hat{\theta}}_i^d = -\frac{\partial \hat{\mathcal{L}}_i}{\partial \hat{\theta}_i^d} + \frac{\sigma}{N} \sum_{j=1}^N a_{ij}(\hat{\theta}_j^d - \hat{\theta}_i^d), \quad (12)$$

with $i \in [1, N]$, $d \in [1, D+1]$ and

$$\frac{\partial \hat{\mathcal{L}}_i}{\partial \hat{\theta}_i^d} = -2\langle \hat{x}_i \hat{y}_i \rangle \prod_{k \neq d}^{D+1} \hat{\theta}_i^k + 2\langle \hat{x}_i^2 \rangle \hat{\theta}_i^d \prod_{k \neq d}^{D+1} (\hat{\theta}_i^k)^2 + 2\gamma \hat{\theta}_i^d, \quad (13)$$

where we use the simplified notation $\langle \cdot \rangle$ to indicate an average (here over the data points assigned to a unit) as we do in the main text. Let us define the local magnetization $m_i = (D+1)^{-1} \sum_d \hat{\theta}_i^d$ as the average learning parameter of the i -th unit and compute the average value of the

gradient in Eq.(13), summing over the different layers, leading to

$$\langle \frac{\partial \hat{\mathcal{L}}_i}{\partial m_i} \rangle \approx -2\langle \hat{x}_i \hat{y}_i \rangle m_i^D + 2\langle \hat{x}_i^2 \rangle m_i^{2D+1} + 2\gamma m_i, \quad (14)$$

where we have used the approximations

$$(D+1)^{-1} \sum_{d=1}^{D+1} (\partial \hat{\mathcal{L}}_i / \partial \hat{\theta}_i^d) \approx \nabla_{m_i} \hat{\mathcal{L}}_i(m_i), \quad (15)$$

$$(D+1)^{-1} \sum_{d=1}^{D+1} \prod_{k \neq d} \hat{\theta}_i^k \approx m_i^D, \quad (16)$$

$$(D+1)^{-1} \sum_{d=1}^{D+1} \hat{\theta}_i^d \prod_{k \neq d} (\hat{\theta}_i^k)^2 \approx m_i^{2D+1}. \quad (17)$$

Now we plug Eq.(14) into the sum of the $(D+1)$ equations in Eq.(12) for each unit. Assuming orthogonal input representations [41, 47] (which holds exactly for whitened input data [41]) we set $\langle \hat{x}_i^2 \rangle = 1$ without loss of generality. After re-scaling time with $dt' = 2dt$ and absorbing any additional constants into the effective variables $\hat{\sigma}$, $\hat{\gamma}$ and $\delta_i = \langle \hat{x}_i \hat{y}_i \rangle$, we get Eq.(4) in the main text.

To derive the mean effective loss of Eq.(5), note from Eq.(11) that the effective output function of a neural unit takes the simple form $\bar{y}_i \approx m_i^{D+1}$. Then, using the MSE as the individual loss function $\ell(\bar{y}_i, y_i)$ –where \bar{y}_i and y_i are both scalars–, the effective loss of the i -th unit when evaluating data assigned to the j -th unit (i.e. the cross-loss entry $(L_x)_{ij}$) becomes

$$(\hat{L}_x)_{ij} = [m_i^{D+1} \hat{x}_j - \hat{y}_j]^2. \quad (18)$$

Decomposing terms, neglecting the constant $\langle \hat{y}_j^2 \rangle$ that depends on the dataset, and assuming again orthogonal input data, we have

$$(\hat{L}_x)_{ij} \sim m_i^{D+1} (m_i^{D+1} - 2\delta_j), \quad (19)$$

which is used as the starting point to estimate the microscopic learning path. Finally, by summing all the entries of this matrix and using that in the test set $\langle \delta \rangle = N^{-1} \sum_j \delta_j$, we get Eq.(5) in the main text.

B. Numerical and experimental details

Effective theory. We integrate the dynamics of Eq.(4) using a RK45 method implemented with a standard SciPy Python solver. At each coupling, we iterate for a time span of 10s, averaging the metrics during the second half of the simulation to discard transient. The number of nodes is set to $N = 200$, regularization is $\hat{\gamma} = 10^{-3}$ and results are averaged over 200 realizations. In the adiabatic protocol, we use the distribution of magnetization from the previous coupling value as the initial condition of the following one, while in the

non-adiabatic protocol we initialize the values at each coupling. The sequence of quenched disorders δ is drawn from a Gaussian distribution $\mathcal{N}(0, 2)$ and the initial condition for the magnetization values is the uniform support in $[-2 + \epsilon, 2 + \epsilon]$, where a small $\epsilon = 0.3$ is used to break the symmetry towards positive solutions of $\langle m \rangle$ in order to reproduce what occurs in the experiments (where the nonlinear neuron activation function always produce $\langle m \rangle > 0$ in the ordered regime).

Dataset. We use the MNIST dataset to validate the effective theory. It consists of 60000 labelled black-and-white images of 28×28 pixels corresponding to handwritten digits from zero to nine, and it is divided into train set (50000) and test set (10000) for cross-validation purposes. The images are flattened as vectors to feed as inputs into the neural network (see below).

Neural architecture. We use standard feed-forward neural networks as the backbone of the neural units. For each data point $x \in \mathbb{R}^{n_0}$, we use $h^d(x) \in \mathbb{R}^{n_d}$ and $x^d(x) \in \mathbb{R}^{n_d}$ for the pre- and post-activation functions. The recurrence relation for a layer of the feed-forward network is defined as

$$h^{d+1} = x^d W^{d+1} + b^{d+1}, \quad x^{d+1} = \phi(h^{d+1}), \quad (20)$$

where $\phi()$ is a point-wise, non-linear activation function (we use the standard ‘ReLU’ function $\phi(x) = \max(0, x)$ [20]), $W^{d+1} \in \mathbb{R}^{n_d \times n_{d+1}}$ is the matrix of weights between layers and $b^{d+1} \in \mathbb{R}^{n_{d+1}}$ is the vector of biases. We define Θ^d as the matrix of layer d that includes both the weights and biases, thus $\Theta^d \in \mathbb{R}^{(n_d+1) \times (n_{d+1}+1)}$. In our simulations, we fix the number of hidden neurons to $n_d = 20$ for all hidden layers and use the Cross-Entropy as the loss function [20], suitable for categorical outputs. The trainable parameters are the entries θ_{ij}^d , initially drawn i.i.d. from $\mathcal{N}(0, 1)$. We also define $\theta = \text{vec}(\cup_{d=1}^{D+1} \Theta^d)$, as the flattened vector of all the parameters of a single neural unit.

Training and evaluation. To minimize the local term in Eq.(2), we use standard Backpropagation with vanilla mini-batch gradient descent (without momentum), with batch size $B = 2^5$. Note that since the batch size is sufficiently large [50], we can neglect an additive noise term that would emerge in Eq. (4) if SGD was used to approximate the global loss function by taking the gradient of a single data point. The learning rate is fixed to $\eta = 0.005$ and weight decay to $\gamma = 10^{-3}$. Results for each coupling value σ are time-averaged during $2 \cdot 10^4$ batch iterations, after $2 \cdot 10^4$ more iterations to discard transient behavior. We run 20 independent realizations of the process, where all parameters are initialized with $\mathcal{N}(0, 1)$ and consider both adiabatic and non-adiabatic protocols.

Acknowledgments: The authors would like to thank S. Ryu, C. Charalambous, J. De Gregorio, J. Moreno, R. Martínez, J. Fernández, P. Colet, M. San Miguel, R.

Toral, C. Granell and A. Arenas for useful discussions. We acknowledge funding from project DYNDEEP (EUR2021-122007) from the Agencia Estatal de Investigación MCIN/AEI/10.13039/501100011033. LL additionally acknowledges funding from project MISLAND (PID2020-114324GB-C22), and María de Maeztu project CEX2021-001164-M.

Code availability: Python scripts (based on PyTorch library) to reproduce the results of the study will be available on github.com/mystic-blue/collective-learning upon publication.

Data availability: All data supporting the results of the study will be available on github.com/mystic-blue/collective-learning upon publication.

-
- [1] P. W. Anderson, More is different, *Science* **177**, 393 (1972).
 - [2] M. Mezard, G. Parisi, and M. Virasoro, *Spin Glass Theory and Beyond* (World Scientific, 1986).
 - [3] S. H. Strogatz, *Sync: The Emerging Science of Spontaneous Order* (Hyperion, New York, 2003).
 - [4] M. A. Muñoz, Colloquium: Criticality and dynamical scaling in living systems, *Rev. Mod. Phys.* **90**, 031001 (2018).
 - [5] R. Solé, M. Moses, and S. Forrest, Liquid brains, solid brains, *Philosophical transactions of the Royal Society of London. Series B, Biological sciences* **374** (2019).
 - [6] J. Piñero and R. Solé, Statistical physics of liquid brains, *Philosophical Transactions of the Royal Society B: Biological Sciences* **374**, 20180376 (2019).
 - [7] D. O. Hebb, *The Organization of Behavior: A Neuropsychological Theory* (John Wiley, New York, USA, 1949).
 - [8] M. J. Mataric, Designing emergent behaviors: From local interactions to collective intelligence, in *Proceedings of the Second International Conference on From Animals to Animats 2* (MIT Press, Cambridge, MA, USA, 1993) p. 432–441.
 - [9] A. Olsson, E. Knapska, and B. Lindström, The neural and computational systems of social learning, *Nature Reviews Neuroscience* **21**, 1 (2020).
 - [10] D. Ha and Y. Tang, Collective intelligence for deep learning: A survey of recent developments, *Collective Intelligence* **1**, 26339137221114874 (2022).
 - [11] J. J. Hopfield, Neural networks and physical systems with emergent collective computational abilities, *Proceedings of the National Academy of Sciences* **79**, 2554 (1982).
 - [12] J. Kennedy and R. Eberhart, Particle swarm optimization, in *Proceedings of ICNN'95 - International Conference on Neural Networks*, Vol. 4 (1995) pp. 1942–1948 vol.4.
 - [13] G. Carleo, I. Cirac, K. Cranmer, L. Daudet, M. Schuld, N. Tishby, L. Vogt-Maranto, and L. Zdeborová, Machine learning and the physical sciences, *Reviews of Modern Physics* **91**, 045002 (2019).
 - [14] M. Mézard, Spin glass theory and its new challenge: structured disorder (2023), [arXiv:2309.06947](https://arxiv.org/abs/2309.06947) [cond-mat.dis-nn].
 - [15] Z. Liu, O. Kitouni, N. S. Nolte, E. Michaud, M. Tegmark, and M. Williams, Towards understanding grokking: An effective theory of representation learning, *Advances in Neural Information Processing Systems* **35**, 34651 (2022).
 - [16] L. Ziyin and M. Ueda, Exact phase transitions in deep learning, [arXiv preprint arXiv:2205.12510](https://arxiv.org/abs/2205.12510) (2022).
 - [17] P. Mehta, M. Bukov, C.-H. Wang, A. G. Day, C. Richardson, C. K. Fisher, and D. J. Schwab, A high-bias, low-variance introduction to machine learning for physicists, *Physics reports* **810**, 1 (2019).
 - [18] D. A. Roberts, S. Yaida, and B. Hanin, *The Principles of Deep Learning Theory* (Cambridge University Press, 2022).
 - [19] S. Mei, T. Misiakiewicz, and A. Montanari, Mean-field theory of two-layers neural networks: dimension-free bounds and kernel limit, in *Conference on Learning Theory* (PMLR, 2019) pp. 2388–2464.
 - [20] I. J. Goodfellow, Y. Bengio, and A. Courville, *Deep Learning* (MIT Press, Cambridge, MA, USA, 2016) <http://www.deeplearningbook.org>.
 - [21] J. Jumper *et al.*, Highly accurate protein structure prediction for the human proteome, *Nature* **596**, 1 (2021).
 - [22] N. Brown and T. Sandholm, Superhuman ai for multi-player poker, *Science* **365**, 885 (2019).
 - [23] S. Bubeck, V. Chandrasekaran, R. Eldan, J. Gehrke, E. Horvitz, E. Kamar, P. Lee, Y. T. Lee, Y. Li, S. Lundberg, *et al.*, Sparks of artificial general intelligence: Early experiments with gpt-4, [arXiv preprint arXiv:2303.12712](https://arxiv.org/abs/2303.12712) (2023).
 - [24] T. Ben-Nun and T. Hoefler, Demystifying parallel and distributed deep learning: An in-depth concurrency analysis, *ACM Comput. Surv.* **52**, 10.1145/3320060 (2019).
 - [25] T. Li, A. K. Sahu, A. S. Talwalkar, and V. Smith, Federated learning: Challenges, methods, and future directions, *IEEE Signal Processing Magazine* **37**, 50 (2019).
 - [26] S. Lee *et al.*, Why m heads are better than one: Training a diverse ensemble of deep networks (2015), [arXiv:1511.06314](https://arxiv.org/abs/1511.06314) [cs.CV].
 - [27] G. M. A. *et al.*, Ensemble deep learning: A review, *Engineering Applications of Artificial Intelligence* **115**, 105151 (2022).
 - [28] P. P. Liang, T. Liu, L. Ziyin, N. B. Allen, R. P. Auerbach, D. Brent, R. Salakhutdinov, and L.-P. Morency, Think locally, act globally: Federated learning with local and global representations, [arXiv preprint arXiv:2001.01523](https://arxiv.org/abs/2001.01523) (2020).
 - [29] H. B. McMahan *et al.*, Communication-efficient learning of deep networks from decentralized data (PMLR, 2017) pp. 1273–1282.
 - [30] J. Wang and G. Joshi, Cooperative sgd: A unified framework for the design and analysis of local-update sgd algorithms, *Journal of Machine Learning Research* **22**, 1 (2021).
 - [31] F. Zhuang, Z. Qi, K. Duan, D. Xi, Y. Zhu, H. Zhu, H. Xiong, and Q. He, A comprehensive survey on transfer learning, *Proceedings of the IEEE* **109**, 43 (2020).
 - [32] J. Lee *et al.*, Wide neural networks of any depth evolve as linear models under gradient descent, in *Proceedings of the 33rd International Conference on Neural Information Processing Systems* (Curran Associates Inc., Red Hook,

- NY, USA, 2019).
- [33] S. Zhang, A. E. Choromanska, and Y. LeCun, Deep learning with elastic averaging sgd, *Advances in neural information processing systems* **28** (2015).
 - [34] S. U. Stich, Local sgd converges fast and communicates little, *ArXiv abs/1805.09767* (2018).
 - [35] B. E. Woodworth, K. K. Patel, and N. Srebro, Mini-batch vs local sgd for heterogeneous distributed learning, *Advances in Neural Information Processing Systems* **33**, 6281 (2020).
 - [36] X. Li, Z. Song, R. Tao, and G. Zhang, A convergence theory for federated average: Beyond smoothness, in *2022 IEEE International Conference on Big Data (Big Data)* (IEEE, 2022) pp. 1292–1297.
 - [37] B. Huang *et al.*, FL-NTK: A neural tangent kernel-based framework for federated learning convergence analysis, *CoRR abs/2105.05001* (2021), 2105.05001.
 - [38] X. Li, K. Huang, W. Yang, S. Wang, and Z. Zhang, On the convergence of fedavg on non-iid data, *arXiv preprint arXiv:1907.02189* (2019).
 - [39] C. Baldassi *et al.*, Unreasonable effectiveness of learning neural networks: From accessible states and robust ensembles to basic algorithmic schemes, *Proceedings of the National Academy of Sciences* **113**, E7655 (2016).
 - [40] C. Baldassi, F. Pittorino, and R. Zecchina, Shaping the learning landscape in neural networks around wide flat minima, *Proceedings of the National Academy of Sciences* **117**, 161 (2020), <https://www.pnas.org/doi/pdf/10.1073/pnas.1908636117>.
 - [41] A. M. Saxe, J. L. McClelland, and S. Ganguli, Exact solutions to the nonlinear dynamics of learning in deep linear neural networks, in *2nd International Conference on Learning Representations, ICLR 2014, Banff, AB, Canada, April 14-16, 2014, Conference Track Proceedings* (2014).
 - [42] C. Van den Broeck, J. Parrondo, J. Armero, and A. Hernández-Machado, Mean field model for spatially extended systems in the presence of multiplicative noise, *Physical Review E* **49**, 2639 (1994).
 - [43] J. Buceta, J. M. Parrondo, and F. Rubia, Random ginzburg-landau model revisited: Reentrant phase transitions, *Physical review. E, Statistical, nonlinear, and soft matter physics* **63**, 031103 (2001).
 - [44] R. Toral, C. J. Tessone, and J. M. V. P. Lopes, Collective effects induced by diversity in extended systems, *The European Physical Journal Special Topics* **143**, 59 (2006).
 - [45] N. Komin, L. Lacasa, and R. Toral, Critical behavior of a ginzburg-landau model with additive quenched noise, *Journal of Statistical Mechanics: Theory and Experiment* **2010**, P12008 (2010).
 - [46] P. Hohenberg and A. Krekhov, An introduction to the ginzburg-landau theory of phase transitions and nonequilibrium patterns, *Physics Reports* **572**, 1 (2014).
 - [47] A. Jacot, F. Gabriel, and C. Hongler, Neural tangent kernel: Convergence and generalization in neural networks, in *Proceedings of the 32nd International Conference on Neural Information Processing Systems, NIPS'18* (Curran Associates Inc., Red Hook, NY, USA, 2018) p. 8580–8589.
 - [48] C. H. Martin and M. W. Mahoney, Implicit self-regularization in deep neural networks: Evidence from random matrix theory and implications for learning, *Journal of Machine Learning Research* **22**, 1 (2021).
 - [49] A. Achille, M. Rovere, and S. Soatto, Critical learning periods in deep neural networks (2019), *arXiv:1711.08856 [cs.LG]*.
 - [50] A. Sclocchi and M. Wyart, On the different regimes of stochastic gradient descent (2023), *arXiv:2309.10688 [cs.LG]*.
 - [51] E. Ott and T. Antonsen, Low dimensional behavior of large systems of globally coupled oscillators, *Chaos (Woodbury, N.Y.)* **18**, 037113 (2008).
 - [52] C. Bick *et al.*, Understanding the dynamics of biological and neural oscillator networks through exact mean-field reductions: a review, *The Journal of Mathematical Neuroscience* **10** (2020).
 - [53] G. Gottwald, Model reduction for networks of coupled oscillators, *Chaos* **25** (2015).
 - [54] L. Arola-Fernández, P. S. Skardal, and A. Arenas, Geometric unfolding of synchronization dynamics on networks, *Chaos* **31**, 061105 (2021).
 - [55] M. Newman, *Networks: An Introduction* (Oxford University Press, Inc., New York, NY, USA, 2010).
 - [56] J. Gómez-Gardeñes *et al.*, Explosive synchronization transitions in scale-free networks, *Phys. Rev. Lett.* **106**, 128701 (2011).
 - [57] P. S. Skardal, J. G. Restrepo, and E. Ott, Frequency assortativity can induce chaos in oscillator networks, *Phys. Rev. E* **91**, 060902 (2015).
 - [58] L. Arola-Fernández *et al.*, Emergence of explosive synchronization bombs in networks of oscillators, *Communication Physics* **5**, 10.1038/s42005 (2022).
 - [59] K. Chatterjee, D. Zufferey, and M. A. Nowak, Evolutionary game dynamics in populations with different learners, *Journal of Theoretical Biology* **301**, 161 (2012).
 - [60] D. Gao, X. Yao, and Q. Yang, A survey on heterogeneous federated learning (2022), *arXiv:2210.04505 [cs.LG]*.
 - [61] J. Gómez-Gardeñes, D. Soriano-Paños, and A. Arenas, Critical regimes driven by recurrent mobility patterns of reaction-diffusion processes in networks, *Nature Physics* **14** (2018).
 - [62] R. Vinuesa, H. Azizpour, I. Leite, M. Balaam, V. Dignum, S. Domisch, A. Felländer, S. D. Langhans, M. Tegmark, and F. Fuso Nerini, The role of artificial intelligence in achieving the sustainable development goals, *Nature communications* **11**, 1 (2020).